# Giant piezoelectricity of monolayer group IV monochalcogenides: SnSe, SnS, GeSe, and GeS

Ruixiang Fei,[1] Wenbin Li,[2] Ju Li,[3] and Li Yang[1,a)]
[1]*Department of Physics, Washington University, St. Louis, Missouri 63130, USA*
[2]*Research Laboratory of Electronics, Massachusetts Institute of Technology, Cambridge, Massachusetts 02139, USA*
[3]*Department of Nuclear Science and Engineering and Department of Materials Science and Engineering, Massachusetts Institute of Technology, Cambridge, Massachusetts 02139, USA*

(Received 28 July 2015; accepted 16 October 2015; published online 27 October 2015)

We predict enormous, anisotropic piezoelectric effects in intrinsic monolayer group IV monochalcogenides (MX, M=Sn or Ge, X=Se or S), including SnSe, SnS, GeSe, and GeS. Using first-principle simulations based on the modern theory of polarization, we find that their piezoelectric coefficients are about one to two orders of magnitude larger than those of other 2D materials, such as $MoS_2$ and GaSe, and bulk quartz and AlN which are widely used in industry. This enhancement is a result of the unique "puckered" $C_{2v}$ symmetry and electronic structure of monolayer group IV monochalcogenides. Given the achieved experimental advances in the fabrication of monolayers, their flexible character, and ability to withstand enormous strain, these 2D structures with giant piezoelectric effects may be promising for a broad range of applications such as nano-sized sensors, piezotronics, and energy harvesting in portable electronic devices. © *2015 AIP Publishing LLC*.
[http://dx.doi.org/10.1063/1.4934750]

Piezoelectric materials, which convert mechanical energy to electrical energy, have the advantages of large power densities and ease of application in sensors and energy harvesting.[1,2] For example, a widely used piezoelectric material is lead zirconate titanate $Pb[Zr_xTi_{1-x}]O_3$, a piezoceramic known as PZT.[3–5] However, the piezoceramic's brittle nature causes limitations in the sustainable strain.[6] Meanwhile, non-centrosymmetric wurtzite-structured semiconductors, such as ZnO, GaN, and InN, are wildly used in the piezotronic and piezo-phototronic devices.[7–9] In particular, their nanowires or nanobelts[10–12] are expected to be useful for electromechanical coupled sensors, nanoscale energy conversion.[10–13] However, the much smaller piezoelectric coefficients of wurtzite semiconductors limit the mechanical-electrical energy conversion efficiency.[7,8]

Recently, two-dimensional (2D) materials have sparked interest for the piezoelectric applications because of their high crystallinity and ability to withstand enormous strain. For those hexagonal structures with a $D_{6h}$ point group, such as boron nitride (*h*-BN) and many transition-metal dichalcogenides (TMDCs), as well as layered orthorhombic structure with a $D_{4h}$ point group, such as group-III monochalcogenides, their symmetry is reduced to the $D_{3h}$ group when thinned down to monolayer. This breaks the inversion symmetry, as shown in Figs. 1(a) and 1(b), giving rise to piezoelectricity. They were predicted to be intrinsically piezoelectric,[14–21] and this idea has been demonstrated by experiments on the $MoS_2$ monolayer.[22–24] Unfortunately, the piezoelectric effect is rather small, e.g., the measured piezoelectric coefficient $e_{11}$ of monolayer $MoS_2$ is only around $2.9 \times 10^{-10}$ C/m,[23] and the mechanical-electrical energy conversion rate is limited to be about 5%.[22]

Therefore, finding flexible, stable, and efficient 2D piezoelectric materials is crucial. This motivates us to study another family of 2D semiconductors, group IV monochalcogenides (MX, M=Sn or Ge, M=Se or S), i.e., SnSe, SnS, GeSe, and GeS. Their atomic structure is presented in Figs. 1(c) and 1(d), which exhibit a $C_{2v}$ point group. We expect an enhanced piezoelectricity due to the following reasons: (1) As shown in Fig. 1(c), their stable monolayer structures are non-centrosymmetric, allowing them to be piezoelectric. (2) Their puckered $C_{2v}$ symmetries are much more flexible (softer) along the armchair direction. This can further enhance the piezoelectric. (3) Significant advances in fabrication techniques have been achieved. For example, few-layer SnSe has been fabricated recently.[25]

In this letter, we employ the first-principles density functional theory (DFT) simulations to calculate the piezoelectric effects of monolayer group-IV monochalcogenides. The piezoelectric effect of these monolayer materials is dramatically enhanced and anisotropic, and the most important piezoelectric coefficient $d_{11}$ is about two orders of magnitude larger than that of 2D and bulk materials,[7,14,16] which have been widely used in the industry. These anisotropic, giant piezoelectric materials represent a new class of nanomaterials that will allow for the next generation of ultra-sensitive mechanical detectors, energy conversion devices, and consumer-touch sensors.

The DFT calculations with the Perdew-Burke-Ernzerh (PBE) functional[26] have been carried out by using the Vienna Ab initio Simulation Package (VASP) with a plane wave basis set[27,28] and the projector-augmented wave method.[29] The Brillouin zone integration is obtained by a $14 \times 14 \times 1$ k-point grid. The convergence criteria for electronic and ionic relaxations are $10^{-6}$ eV and $10^{-3}$ eV/Å, respectively. We use the "Berry-phase" theory of polarization to directly compute the electric polarization.[30–32] The change of polarization ($\Delta P$)

a)Author to whom correspondence should be addressed. Electronic mail: lyang@physics.wustl.edu

 

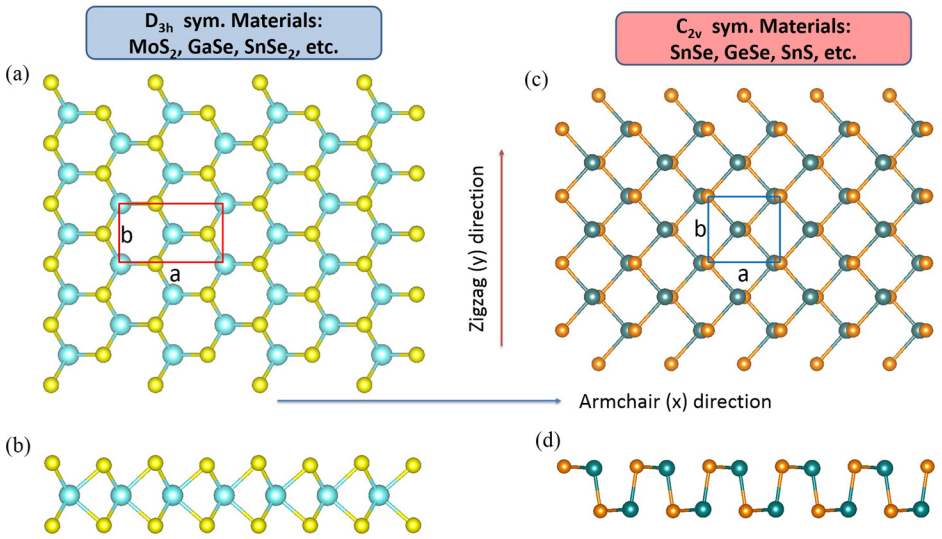


FIG. 1. The ball-stick atomic structure of $D_{3h}$ hexagonal and $C_{2v}$ orthorhombic monolayers. (a) and (b) The side top and side views of the hexagonal monolayer. (c) and (d) The top and side views of the orthorhombic monolayer. The armchair direction and zigzag direction are defined as the x and y directions, respectively.

occurs upon making an adiabatic change in the Kohn-Sham Hamiltonian of the crystal.

The DFT-optimized monolayer and bulk structure parameters, i.e., the in-plane lattice constants $a$ and $b$, are listed in Table I. The corresponding experimental or the previous DFT results of the bulk phase are listed as well.[33–42] We observe a similar trend as that in Ref. 42, in which the lattice constant $a$ increases and the constant $b$ decreases with increasing the number of layers for most group IV monochalcogenides, except for GeS. These monolayers are metastable. This is evidenced by recent experimental fabrications[25] and theoretical phonon calculations.[43]

We have calculated the electronic structure of group IV monochalcogenides in the supplementary material.[44] All these materials exhibit an indirect band gap at the DFT level. We list the values of band gaps in Table I. These DFT gap values are for reference purposes only, as excited-state calculations are needed to get the reliable band gap of MXs. According to our experience,[45,46] the quasiparticle band gaps of MX range from 1.2 eV to 2.7 eV, which are within a very useful range for electronic applications. Moreover, huge excitonic effects are expected, which can substantially lower the optical absorption edge, promising for solar energy applications.[25,47]

Fortunately, piezoelectric properties are ground-state properties and the DFT calculation is a suitable tool shown to reliably predict the values. For example, the DFT-calculated piezoelectric coefficients are in excellent agreement with the experimental values for the bulk GaN.[48] Very recently, experiments measured the piezoelectric coefficient $e_{11} = 2.9 \times 10^{-10}$ C/m for monolayer $MoS_2$, which is close to the DFT results ($3.6 \times 10^{-10}$ C/m).[14,23] Therefore, we employ the same theoretical approach in this work.

We first obtained the planar elastic stiffness coefficients $C_{11}$, $C_{22}$, and $C_{12}$ of the MX monolayer by fitting the DFT-calculated unit-cell energy $U$ to a series of 2D strain states ($\varepsilon_{11}$,$\varepsilon_{22}$), based on the formula

$$C_{11} = \frac{1}{A_0}\frac{\partial^2 U}{\partial \varepsilon_{11}^2}, \; C_{22} = \frac{1}{A_0}\frac{\partial^2 U}{\partial \varepsilon_{22}^2}, \; C_{12} = \frac{1}{A_0}\frac{\partial^2 U}{\partial \varepsilon_{11}\partial \varepsilon_{22}}, \quad (1)$$

where $A_0$ is the unit-cell area at the zero strain. Due to the existence of mirror symmetry along the zigzag direction (y direction), at the small strain limit, we can write

$$\Delta u(\varepsilon_{11}, \varepsilon_{22}) = \frac{1}{2}C_{11}\varepsilon_{11}^2 + \frac{1}{2}C_{22}\varepsilon_{22}^2 + C_{12}\varepsilon_{11}\varepsilon_{22}, \quad (2)$$

where $\Delta u(\varepsilon_{11}, \varepsilon_{22}) = [U(\varepsilon_{11}, \varepsilon_{22}) - U(\varepsilon_{11}=0, \varepsilon_{22}=0)]/A_0$ is the change of unit-cell energy per area. We carry out the strain energy calculation on an $11 \times 11$ grid with $\varepsilon_{11}$ and $\varepsilon_{22}$ ranging from $-0.005$ to 0.005. The atomic positions in the strained unit cell are allowed to be fully relaxed. Following the definitions of previous works,[23] the coefficients $C_{11}$, $C_{22}$, and $C_{12}$, which are calculated using a fully relaxed atomic configuration, are called relaxed-ion stiffness coefficients, which are experimentally relevant. In contrast, if the atomic positions are held when applying strain, the so-called clamped-ion coefficients, which represent the piezoelectric effect from the electronic contribution,[49] can be calculated as well.

Table II summarizes the clamped and relaxed-ion stiffness coefficients for the four types of $C_{2v}$ symmetry MX

TABLE I. Experimental and DFT-PBE calculated structural parameters and bandgap for bulk and monolayer MX. The values of monolayer lattice constants $a$ and $b$, direct and indirect bandgaps are listed.

| | Monolayer DFT calculation | | | | Bulk experiment or DFT calculation | | | |
|---|---|---|---|---|---|---|---|---|
| Material | a (Å) | b (Å) | Indirect gap (eV) | Direct gap (eV) | a (Å) | b (Å) | Indirect gap (eV) | Direct gap (eV) |
| GeS | 4.48 | 3.62 | 1.23 | 1.36 | 4.30[33] exp. | 3.64[33] exp. | 1.58[34] exp. | 1.61[34] exp. |
| GeSe | 4.27 | 3.93 | 1.04 | 1.10 | 4.38[35] exp. | 3.82[35] exp. | 1.16[36] exp. | 1.53[36] exp. |
| SnS | 4.26 | 4.03 | 1.37 | 1.51 | 4.33[37] exp. | 3.99[37] exp. | 1.07[38] theory | 1.3[39] exp. |
| SnSe | 4.35 | 4.24 | 0.77 | 0.92 | 4.44[40] exp. | 4.14[40] exp. | 0.86[40] exp. | 1.30[41] theory |

monolayers. Additionally, we have also listed the elastic stiffness of another two typical $D_{3h}$ symmetry piezoelectric materials, $MoS_2$[14] and GaSe.[16] According to the structures shown in Figs. 1(c) and 1(d), group IV monochalcogenides are soft along the armchair (x) direction. This is consistent with our DFT results in Table II. In particular, for both clamped and relax-ion cases, the elastic stiffnesses ($C_{11}$) of group-IV monochalcogenide are about 4–6 times smaller than that of $MoS_2$ and GaSe. This will significantly enhance the piezoelectric effects. An unexpected result from Table II is that the elastic stiffness ($C_{22}$) along the zigzag (y) direction is also substantially smaller (around 2–3 times) than that of $MoS_2$ and GaSe. This may be attributed to the intrinsic electronic properties of group IV monochalcogenides, whose covalence bonds are weaker than those of hexagonal TMDCs and group III monochalcogenides. This is also reflected in their longer bond lengths (2.50–2.89 Å), compared with those of GaSe (2.47 Å) and $MoS_2$ (1.84 Å).[14,16]

Recently, puckered 2D structures, such as few-layer black phosphorus (phosphorene) and similar isoelectronic materials,[50] have attracted significant research interests. Due to their novel structure, phosphorene exhibits an unusually negative Poisson ratio.[51] Here, we have calculated the Poisson ratio $\nu\perp$ obtained directly from relaxed ion coordinates by evaluating the change of layer thickness in response to in-plane hydrostatic strain $\Delta h/h = -\nu_{\perp}(\varepsilon_{11}+\varepsilon_{22})$. The Poisson ratio $\nu\perp$ is investigated by averaging the results of the armchair direction and zigzag direction for small stress (−0.8%–0.8%). Interestingly, our calculated value is positive and similar to those of the TMDCs and group III monochalcogenides. This differs from the result of phosphorene, in which the Poisson ratio is evaluated by the value only from the armchair direction within a much larger stress range (−5%–5%).[51]

Next, we calculated the linear piezoelectric coefficients of the group IV MX monolayers by evaluating the change of unit-cell polarization after imposing uniaxial strain. The linear piezoelectric coefficients $e_{ijk}$ and $d_{ijk}$ are third-rank tensors as they relate polarization vector $P_i$, to strain $\varepsilon_{jk}$ and stress $\sigma_{jk}$, respectively,

$$e_{ijk} = \frac{\partial P_i}{\partial \varepsilon_{jk}}, \tag{3}$$

TABLE II. DFT-PBE calculated in-plane elastic stiffness $C_{11}$, $C_{22}$, and $C_{12}$ of monolayer group IV monochalcogenides. The Poisson ratio $\nu_{\perp}$ is calculated for the relaxed ion case. The data of a typical TCMD monolayer material, $MoS_2$, and a typical group III monochalcogenide, GaSe, are listed for reference as well.

| | Clamp-ion | | | Relax-ion | | | |
|---|---|---|---|---|---|---|---|
| Material | $C_{11}$ (N/m) | $C_{22}$ (N/m) | $C_{12}$ (N/m) | $C_{11}$ (N/m) | $C_{22}$ (N/m) | $C_{12}$ (N/m) | $\nu_{\perp}$ |
| GeS | 48.90 | 58.19 | 32.92 | 20.87 | 53.40 | 22.22 | 0.32 |
| GeSe | 43.76 | 56.16 | 31.18 | 13.81 | 46.62 | 17.49 | 0.35 |
| SnS | 45.79 | 52.49 | 33.46 | 14.91 | 35.97 | 15.22 | 0.36 |
| SnSe | 43.96 | 47.60 | 30.66 | 19.88 | 44.49 | 18.57 | 0.42 |
| $MoS_2$[14] | 153 | 153 | 48 | 130 | 130 | 32 | 0.34 |
| GaSe[16] | 108 | 108 | 32 | 83 | 83 | 18 | 0.39 |

$$d_{ijk} = \frac{\partial P_i}{\partial \sigma_{jk}}. \tag{4}$$

Because of the mirror symmetry along the zigzag (y) direction, the independent piezoelectric coefficients are $\{e_{111}, e_{122}, e_{212}=e_{221}\}$ and $\{d_{111}, d_{122}, d_{212}=d_{221}\}$. Indices 1 and 2 correspond to the *x* and *y* directions, respectively. The reason that $e_{212}=e_{221}$ and $d_{212}=d_{221}$ is because the strain tensor is usually defined to be symmetric, namely, $\varepsilon_{jk}=\varepsilon_{kj}$. The piezoelectric coefficients $e_{212}$ and $d_{212}$ describe the response of polarization to shear strain $\varepsilon_{12}$. In the following, we particularly focused on $\{e_{111}, e_{122}\}$ and $\{d_{111}, d_{122}\}$, as well as the relationship between the $e_{ijk}$ and $d_{ijk}$.

By definition, the tensors are related by

$$e_{ijk} = \frac{\partial P_i}{\partial \varepsilon_{jk}} = \frac{\partial P_i}{\partial \sigma_{mn}}\frac{\partial \sigma_{mn}}{\partial \varepsilon_{jk}} = d_{imn}C_{mnjk}, \tag{5}$$

where $C_{mnjk}$ are elastic constants. In 2D structures, an index can be either 1 or 2. Therefore,

$$e_{111} = d_{111}C_{1111} + d_{122}C_{2211}, \tag{6}$$

$$e_{122} = d_{111}C_{1122} + d_{122}C_{2222}. \tag{7}$$

Using the Voigt notation, we simplify it as $e_{11}=e_{111}$, $e_{12}=e_{122}$, $d_{11}=d_{111}$, $d_{12}=d_{122}$, $C_{11}=C_{1111}$, $C_{12}=C_{1122}=C_{2211}$. Then, we calculated $d_{11}$ and $d_{12}$ by $e_{11}$ and $e_{12}$ as

$$d_{11} = \frac{e_{11}C_{22} - e_{12}C_{12}}{C_{11}C_{22} - C_{12}^2}, \tag{8}$$

$$d_{12} = \frac{e_{12}C_{11} - e_{11}C_{12}}{C_{11}C_{22} - C_{12}^2}. \tag{9}$$

We have directly calculated the polarization of the MX monolayers by applying the uniaxial strain $\varepsilon_{11}$ and $\varepsilon_{22}$ to the orthorhombic unit cell along the x and y directions, respectively. The change of polarization along the y direction is zero, because the mirror symmetry still remains under an uniaxial strain for the $C_{2v}$ point group. The values of $e_{11}$ and $e_{12}$ are evaluated by a linear fit of 2D unit-cell polarization change along the x direction ($\Delta P_1$) with respect to $\varepsilon_{11}$ and $\varepsilon_{22}$. In Figs. 2(a) and 2(b), we use $\varepsilon_{11}$ and $\varepsilon_{22}$ ranging from −0.005 to 0.005 in steps of 0.001 in the champed-ion case and −0.01–0.01 in steps of 0.002 in the relax-ion case. The dense steps of 0.001 are required for monolayer SnSe and SnS because their linear polarization changes occurring in the strain region are very small, less than ±0.004, as shown in Figs. 2(c) and 2(d). For $e_{11}$, the trend of polarization vs. strain is different for the cases of GeS and GeSe, and for $e_{12}$, the trend is different for SnSe and SnS. This is because of the competition between ionic polarization contribution and electron polarization for $e_{11}$ of GeS and GeSe, and $e_{12}$ of SnS and SnSe. The relaxed-ion (or clamped-ion) $d_{11}$ and $d_{12}$ coefficients are finally calculated by the corresponding $e_{11}$, $e_{12}$ coefficients and elastic stiffness coefficients $C_{11}$, $C_{22}$, and $C_{12}$ based on Eqs. (8) and (9).

We have summarized the calculated $e_{11}$, $e_{12}$, $d_{11}$, and $d_{12}$ coefficients in Table III. The most useful piezoelectric coefficients (relaxed-ion $d_{11}$ and $d_{12}$), which reflect how much polarization charge can be generated with a fixed force

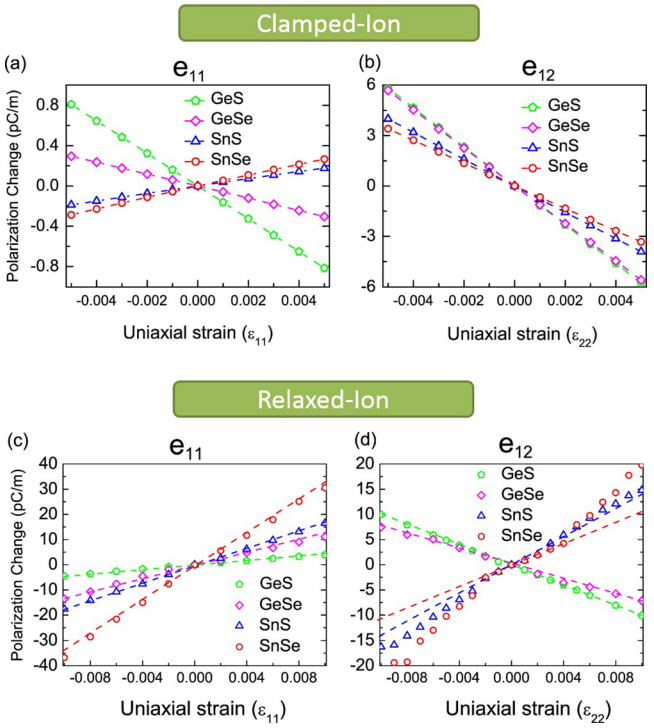


FIG. 2. Change of unit-cell polarization per area of the MX monolayers along the x direction after applying uniaxial strain $\varepsilon_{11}$ (a) and (c) and $\varepsilon_{22}$ (b) and (d). The piezoelectric coefficients $e_{11}$ and $e_{12}$ correspond to the slope of lines obtained through linear fitting of polarization change with respect to $\varepsilon_{11}$ and $\varepsilon_{22}$.

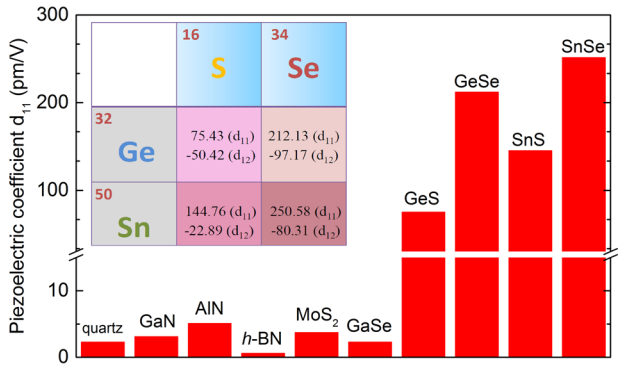


FIG. 3. Comparison of the characteristic piezoelectric coefficient ($d_{11}$) between previously known piezoelectric materials and our proposed group IV monochalcogenides. A break in the y-axis is necessary to make previously studied materials visible. The inset shows the trends of relaxed-ion structural, elastic, and piezoelectric properties.

and thus decide the mechanic-electrical energy converting ratio, are about 75–250 pm/V. Compared with those of frequently used bulk piezoelectric materials, such as α-quartz, wurtzite AlN, and ZnO,[7,14,52–54] and recently emerging 2D piezoelectric materials, such as $MoS_2$ and GaSe,[14,16,23] these values are about two orders of magnitude larger, as shown in Fig. 3.

Finally, we find that the relaxed-ion $d_{11}$ and $d_{12}$ coefficients in the MX monolayers obey a periodic trend, as shown in the inset of Fig. 3. GeS possesses the smallest piezoelectric effect ($d_{11} = 75.43$ pm/V and $d_{12} = -50.42$ pm/V), and moving upward in groups 14 (crystallogens) and 16 (chalcogenide) enhances the magnitude of the effect until SnSe, which has the largest coefficient ($d_{11} = 250.58$ pm/V, $d_{12} = -80.31$ pm/V), is reached. Interestingly, this trend is similar to that discovered in the hexagonal TMDCs.[14] More calculations on similar puckered $C_{2v}$ symmetry materials may be necessary to conclude the interesting trend of piezoelectric effects revealed in those honeycomb structures.[18]

These group IV monochalcogenides have highly desirable properties useful for a broad range of applications. On the other hand, for realistic devices, many other factors, in addition to the piezoelectric coefficients, will need to be considered. For instance, substrate effects and carrier mobilities are important for deciding the converting ratio in energy capture devices and the mechanical fatigue of these flexible materials has not been tested yet. It is also known that the layer number may dramatically impact the piezoelectric effect.[22] These are beyond the scope of this letter, but further research is expected.

By reliable simulations, we have demonstrated that monolayer group IV monochalcogenides MX, GeS, GeSe, SnS, and SnSe are strongly piezoelectric. Their piezoelectric coefficients are surprisingly one to two orders of magnitude larger than other frequently used piezoelectric materials. Encouraged by experimental achievements of monolayer samples, we expect that the huge piezoelectric properties of these materials to provide new platforms for electronic and piezotronic devices, and enable previously inaccessible avenues for sensing and control at the nanoscale.

TABLE III. Calculated clamped-ion and relaxed-ion piezoelectric coefficients, $e_{11}$, $e_{12}$, $d_{11}$, and $d_{12}$.

| | Clamp-ion | | | | Relax-ion | | | |
|---|---|---|---|---|---|---|---|---|
| Material | $e_{11}$ $10^{-10}$ C/m | $e_{12}$ $10^{-10}$ C/m | $d_{11}$ (pm/V) | $d_{12}$ (pm/V) | $e_{11}$ $10^{-10}$ C/m | $e_{12}$ $10^{-10}$ C/m | $d_{11}$ (pm/V) | $d_{12}$ (pm/V) |
| GeS | −1.62 | −11.6 | 16.39 | −29.21 | 4.6 | −10.1 | 75.43 | −50.42 |
| GeSe | −0.62 | −11.0 | 20.75 | −31.11 | 12.3 | −8.2 | 212.13 | −97.17 |
| SnS | 0.36 | −7.9 | 22.07 | −29.12 | 18.1 | 13.8 | 144.76 | −22.89 |
| SnSe | 0.65 | −6.68 | 20.46 | −27.21 | 34.9 | 10.8 | 250.58 | −80.31 |
| Bulk α-quartz | | | | | | | 2.3[53] exp. | |
| Bulk AlN (wurtzite) | | | | | | | 5.1 (d33)[54] exp. | |
| ZnO | | | | | 0.89 ($e_{33}$)[7] theory | −0.51 ($e_{31}$)[7] theory | 9.93 (d33)[52] exp. | |
| $MoS_2$ | | | | | 3.64[14] theory 2.9[23] exp. | | 3.73[14] theory | |
| GaSe | 5.22[16] theory | | 9.67[16] theory | | 1.47[16] theory | | 2.3[16] theory | |

We acknowledge the fruitful discussions with Vy Tran and Anders Carlsson. R. Fei and L.Y. were supported by the National Science Foundation (NSF) Grant No. DMR-1207141 and NSF CAREER Grant No. DMR-1455346. J.L. and W.B.L. acknowledge the support by NSF DMR-1410636 and DMR-1120901. The computational resources have been provided by the Stampede of Teragrid at the Texas Advanced Computing Center (TACC) through XSEDE.

[1]A. Erturk and D. J. Inman, *Piezoelectric energy harvesting* (John Wiley & Sons, 2011).
[2]K. A. Cook-Chennault, N. Thambi, and A. M. Sastry, Smart Mater. Struct. **17**, 043001 (2008).
[3]A. I. Kingon and S. Srinivasan, Nat. Mater. **4**, 233–237 (2005).
[4]S. Xu, B. J. Hansen, and Z. L. Wang, Nat. Commun. **1**, 93 (2010).
[5]T. D. Nguyen, N. Deshmukh, J. M. Nagarah, T. Kramer, P. K. Purohit, M. J. Berry, and M. C. McAlpine, Nat. Nanotechnol. **7**, 587–593 (2012).
[6]S. R. Anton and H. A. Sodano, Smart Mater. Struct. **16**, R1 (2007).
[7]F. Bernardini, V. Fiorentini, and D. Vanderbilt, Phys. Rev. Lett. **79**, 3958 (1997).
[8]I. L. Guy, S. Muensit, and E. M. Goldys, Appl. Phys. Lett. **75**, 4133–4135 (1999).
[9]Z. L. Wang, Adv. Mater. **24**, 4632–4646 (2012).
[10]Z. L. Wang and J. Song, Science **312**, 242–246 (2006).
[11]C. Pan, L. Dong, G. Zhu, S. Niu, R. Yu, Q. Yang, Y. Liu, and Z. L. Wang, Nat. Photonics **7**, 752–758 (2013).
[12]X. Wang, J. Zhou, J. Song, J. Liu, N. Xu, and Z. L. Wang, Nano Lett. **6**, 2768–2772 (2006).
[13]S. Xu, Y. Qin, C. Xu, Y. Wei, R. Yang, and Z. L. Wang, Nat. Nanotechnol. **5**, 366–373 (2010).
[14]K. A. N. Duerloo, M. T. Ong, and E. J. Reed, J. Phys. Chem. Lett. **3**, 2871–2876 (2012).
[15]K. H. Michel and B. Verberck, Phys. Rev. B **80**, 224301 (2009).
[16]W. Li and J. Li, "Piezoelectricity in two-dimensional group III monochalcogenides," preprint arXiv:150307379 (2015).
[17]Z. Chang, W. Yan, J. Shang, and J. Z. Liu, Appl. Phys. Lett. **105**, 023103 (2014).
[18]M. N. Blonsky, H. L. Zhuang, A. K. Singh, and R. G. Hennig, "Ab Initio Prediction of Piezoelectricity in Two-Dimensional Materials," ACS Nano (to be published).
[19]H. L. Zhuang and R. G. Hennig, Chem. Mater. **25**, 3232–3238 (2013).
[20]M. T. Ong and E. J. Reed, ACS Nano **6**, 1387–1394 (2012).
[21]H. L. Zhuang, M. D. Johannes, M. N. Blonsky, and R. G. Hennig, Appl. Phys. Lett. **104**, 022116 (2014).
[22]W. Wu, L. Wang, Y. Li, F. Zhang, L. Lin, S. Niu, D. Chenet, X. Zhang, Y. Hao, T. F. Heinz, J. Hone, and Z. L. Wang, Nature **514**, 470–474 (2014).
[23]H. Zhu, Y. Wang, J. Xiao, M. Liu, S. Xiong, Z. J. Wong, Z. Ye, Y. Ye, X. Yin, and X. Zhang, Nat. Nanotechnol. **10**, 151–155 (2015).
[24]J. Qi, Y. W. Lan, A. Z. Stieg, J. H. Chen, Y. L. Zhong, L. J. Li, C. D. Chen, Y. Zhang, and K. L. Wang, Nat. Commun. **6**, 7430 (2015).
[25]L. Li, Z. Chen, Y. Hu, X. Wang, T. Zhang, W. Chen, and Q. Wang, J. Am. Chem. Soc. **135**, 1213–1216 (2013).
[26]J. P. Perdew, K. Burke, and M. Ernzerhof, Phys. Rev. Lett. **77**, 3865 (1996).
[27]G. Kresse and J. Furthmüller, Comput. Mater. Sci. **6**, 15–50 (1996).
[28]G. Kresse and J. Furthmüller, Phys. Rev. B **54**, 11169 (1996).
[29]P. E. Blöchl, Phys. Rev. B **50**, 17953 (1994).
[30]R. D. King-Smith and D. Vanderbilt, Phys. Rev. B **47**, 1651 (1993).
[31]R. Resta and D. Vanderbilt, *Physics of Ferroelectrics: a Modern Perspective* (Springer-Verlag, 2007), pp. 31–68.
[32]D. Vanderbilt, J. Phys. Chem. Solids **61**, 147–151 (2000).
[33]T. Grandke and L. Ley, Phys. Rev. B **16**, 832 (1977).
[34]D. D. Vaughn II, R. J. Patel, M. A. Hickner, and R. E. Schaak, J. Am. Chem. Soc. **132**, 15170–15172 (2010).
[35]Y. Ishihara and I. Nakada, Phys. Status Solidi B **105**, 285–290 (1981).
[36]E. P. O. O'Reilly, J. Phys. C Solid State Phys. **15**, 1449 (1982).
[37]H. Wiedemeier and H. G. V. Schnering, Z. Kristallogr. **148**, 295–303 (1978).
[38]J. Vidal, S. Lany, M. d'Avezac, A. Zunger, A. Zakutayev, J. Francis, and J. Tate, Appl. Phys. Lett. **100**, 032104 (2012).
[39]K. R. Reddy, N. K. Reddy, and R. W. Miles, Sol. Energy Mater. Sol. Cells **90**, 3041–3046 (2006).
[40]L. D. Zhao, S. H. Lo, Y. Zhang, H. Sun, G. Tan, C. Uher, C. Wolverton, V. P. David, and M. G. Kanatzidis, Nature **508**, 373–377 (2014).
[41]I. Lefebvre, M. A. Szymanski, J. Olivier-Fourcade, and J. C. Jumas, Phys. Rev. B **58**, 1896 (1998).
[42]L. C. Gomes and A. Carvalho, Phys. Rev. B **92**, 085406 (2015).
[43]L. C. Zhang, G. Qin, W. Z. Fang, H. J. Cui, Q. R. Zheng, Q. B. Yang, and G. Su, "SnSe monolayer: Super-flexible, auxetic material with ultralow lattice thermal conductivity and ultrahigh hole mobility," preprint arXiv:1505.04590 (2015).
[44]See supplementary material at http://dx.doi.org/10.1063/1.4934750 for band structure of intrinsic GeS, GeSe, SnS, and SnSe.
[45]V. Tran, R. Soklaski, Y. Liang, and L. Yang, Phys. Rev. B **89**, 235319 (2014).
[46]Y. Liang, S. Huang, R. Soklaski, and L. Yang, Appl. Phys. Lett. **103**, 042106 (2013).
[47]M. A. Franzman, C. W. Schlenker, M. E. Thompson, and R. L. Brutchey, J. Am. Chem. Soc. **132**, 4060–4061 (2010).
[48]K. Shimada, Jpn. J. Appl. Phys., Part 2 **45**, L358 (2006).
[49]F. Bernardini, V. Fiorentini, and D. Vanderbilt, Phys. Rev. B **56**, R10024 (1997).
[50]Z. Zhu, J. Guan, D. Liu, and D. Tománek, ACS Nano **9**, 8284 (2015).
[51]J. W. Jiang and H. S. Park, Nat. Commun. **5**, 4727 (2014).
[52]M. H. Zhao, Z. L. Wang, and S. X. Mao, Nano Lett. **4**, 587–590 (2004).
[53]R. Bechmann, Phys. Rev. **110**, 1060–1061 (1958).
[54]C. M. Lueng, H. L. W. Chan, C. Surya, and C. L. Choy, J. Appl. Phys. **88**, 5360 (2000).